Assessment of Blast-Induced Damage in A Hard Rock Blasting

Magreth Dotto, Yashar Pourrahimian, and Tim Joseph
Mining Optimization Laboratory (MOL)
University of Alberta, Edmonton, Canada

ABSTRACT

Explosive energy usage in fragmenting the rock mass is a complicated phenomenon, highly influenced by rock response to higher stresses, higher loading rates, and the presence of discontinuities. The approach is presented to analyze the effects of rock mass properties on explosive energy. It is divided into steps to estimate total blast energy produced, characterize the rock mass, assess failure mechanisms, and the blast-induced damage. Through a case study in an open pit gold mine, the investigation is done on five production shots of variable sizes with over 1300 charged holes to analyze the explosive energy/rock mass interaction. The ratio of in-situ block size to the average fragmentation size is calculated to evaluate the effect of rock mass on energy distribution and fragmentation in variable rock masses.

1. Introduction

Initially, the objective of blasting in an open-pit mine was to get the rock to a manageable size for trucks and shovels while minimizing the cost of drilling and explosives. Recently, the industry has been focusing on studies to improve blast efficiency to reduce comminution costs and increase productivity on mine-to-mill optimization. These studies have shown that it is possible to improve downstream productivity and reduce costs by investing in blasting processes (Kanchibotla et al., 1999; McKee, 2013; Nielsen & Malvik, 1999).

Blast design improvement is a challenging task due to variations in mechanical rock mass properties and rock response to blast energy (higher stresses and loading rates), which are not usually captured in the static laboratory tests performed in the field. Studies to examine blast energy efficiency have considered homogeneous rock mass and static loading assumptions (Hamdi et al., 2008; Lusk & Silva, 2018; Sanchidrián et al., 2007). With way higher breaking strengths, consideration of static strength cannot fully account for the total energy used in blasting. Empirical fragmentation prediction models are the most popular tools currently used in predicting blast fragmentation from the explosive energy, blast design, and rock mass factor (Cunningham, 2005; Ouchterlony, 2005). Although these models are reasonable engineering tools in fragmentation prediction, they do not offer an account of how and why fracturing occurs, the influence of dynamic loading on rock strengths, or the effect of rock mass properties on blast energy.

Blast-induced rock mass damage has been studied for over three decades to improve the understanding and provide theories on the interaction between rock mass and blast energy (Blair & Minchinton, 1997; Sun, 2013; R. Yang et al., 1996). The areas of interest have been the non-ideal

[1]A version of this paper is under review by the CIM Journal

ISBN: 978-1-55195-486-8

detonation of commercial explosives used in blasting, response of rock mass to higher stresses and loading rates, and the effect of structures. Rock mass rating (RMR) has been used to evaluate the rock mass in blast improvement studies (Chakraborty & Jethwa, 1996; Singh & Narendrula, 2007) mainly due to similarities in influencing factors namely rock strength, joints characteristics, and groundwater. Observations made indicate that the intact rock properties and the presence of discontinuities highly influence rock mass behavior, overall energy use, and resulting fragmentation in blasting. Physical and mechanical properties of rock mass govern the detonation efficiency, energy partition, rock mass response to blast energy, and distribution of blast energy within the rock mass, (Brinkmann, 1990; Hamdi & du Mouza, 2005; Mortazavi et al., 2002; Udy & Lownds, 1990). As the energy interacts with the rock mass, rock joints and fractures govern stress wave propagation, gas pressure confinement, and overall fragmentation size distribution (Hamdi & du Mouza, 2005; Lizotte & Scoble, 1994; Zhu et al., 2007).

Blast-induced damage is associated with stress wave peak particle velocity (PPV) whose attenuation on the ground is commonly estimated using scaled distance (ISEE, 2011; R. L. Yang et al., 1994). PPV attenuation depends on the size of the charge per delay, distance from the charge to the monitoring station, burden size, inelastic attenuation index, and the encountered geology. Encountered geology involves rock physical and mechanical properties, geological structures (joints, faults, fissures, bedding planes, fractures, etc.), and topography. Several studies have proposed modified general relationships on ground vibration prediction to take into consideration site encountered geology and burden distance, (Ak & Konuk, 2008; Bilgin et al., 1998; Hao et al., 2001; Kuzu, 2008; Wu et al., 1998). The proposed relations have been used to determine peak value attenuations and spatial variations, and predict blast-induced stress waves.

This paper reviews studies on rock mass/explosive energy interaction and applies combination of the proposed relationships with the actual field measurements to evaluate blast-induced fragmentation. The approach is purely analytical targeting estimation of damage zones around the blastholes and the burden size from the rock mass characterization, the velocity of detonation (VOD), and blast vibration monitoring. The analysis is essential in defining the extent to which explosive energy is effective in causing fracturing and aid blast design in variable rock masses.

2. Blast-Induced Damage

The theory of rock fracture and fragmentation due to blasting suggests an overall combined damage mechanism; where intensity, propagation, and interaction of stress waves are responsible for initially fracturing the rock (conditioning) while the ensuing gas pressure predominantly effects fragmentation breakage and displacement beyond the immediate borehole region. The induced shock front precedes the gas pressure, causing the borehole's initial pulverized zone and dissipating the fracture zone. While the crushed zone is formed due to higher compressive stress after the stress wave travels through a distance and the rock yields, the tangential stress change from compressive to tensile forming radial cracks in the fracture zone (Zhu et al., 2007).

Blast fragmentation is influenced by rock dynamic strength; with increasing confinement and loading rate, the rock can withstand higher forces before failure. Kimberley et al. (2013) observed compressive strength increased up to three times compared to the strength measured at low rates when strain rate was above 100 s^{-1}. Analyzing data from different studies on different rock types, Zhang and Zhao (2014) suggested that dynamic tensile strength in rocks increases sharply above a critical strain 10 s^{-1}. Mohanty (1987) and Cho et al. (2003) observed that dynamic tensile strength is 2 to 12 times higher than static tensile strength for various rock types. For blast events, the strain rate is estimated to be between 10 and 100 s^{-1} (Chitombo et al., 1999; Fleetwood et al., 2009).

The zones around the blasthole are described by Hustrulid (1999) as shown in Figure 1. The velocity of detonation and borehole pressure are primarily used to determine the magnitude of the initial stress available to initiate rock failure over the material strength (ISEE, 2011). Damage potential can be determined if the wave attenuation in the rock mass is known by assuming that the peak particle velocity (PPV) is proportional to dynamic stress experienced by the rock mass (Mojitabai & Beattie, 1996; Onederra & Esen, 2004; Personn, 1997; R. L. Yang et al., 1994).

In fully coupled charges, shock waves produced are transmitted outward from the explosive axis. When the wave impinges the rock, it is subjected to higher stress and fails by plastic deformation. Upon the arrival of the shock wave, the rock status changes from undisturbed to shocked status. The initial rock parameters Po (pressure), u_o (particle velocity), ρ_o (density), v_o (specific volume), and e_o (specific internal energy) changes to shocked states P_1, u_1, ρ_1, v_1, and e_1. Rankine-Hugoniot jump equations considering fundamental laws of physics for energy, mass, and momentum conservations in Equations (1, 2, and 3) can be used to formulate shock discontinuity propagation in the rock, (Cooper, 1996; Henrych, 1979).

From the law of energy conversation

$$e_1 - e_0 = \frac{1}{2}\left(P_1 + P_0\right)\left(v_0 - v_1\right) \tag{1}$$

Mass equation

$$\frac{\rho_1}{\rho_0} = \frac{v_0}{v_1} = \frac{VOD}{VOD - u_1} \tag{2}$$

Momentum conservation

$$P_1 - P_0 = \rho_0\left(u_1 - u_0\right)\left(VOD - u_0\right) \tag{3}$$

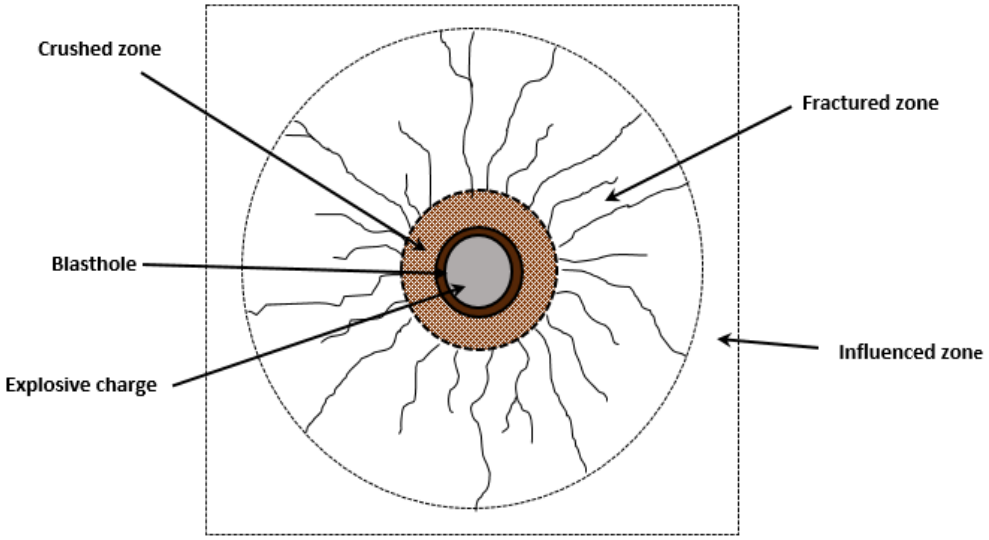

Figure 1. Zones around a blasthole.

Internal energy can be calculated from Equation (4). γ is an isentropic exponent with values ranging from $2.54 \leq \gamma \leq 3$ depending on the kind of explosive (Henrych, 1979). The particle velocity at the interface (u_r) and shock pressure at the rock interface (P_r) for fully coupled cylindrical charges were derived by Liu and Katsabanis (1993) and (Liu & Tidman, 1995) in Equations (5) and (6) assuming an adiabatic process and constant rock density in front of the shock front. P_d is the detonation pressure and V_r is the shock velocity in rock interface, which is estimated by Hugoniot equation (7), Cooper (1996).

$$e = \frac{P(v)}{\gamma + 1} \tag{4}$$

$$u_r = \frac{2VOD}{\gamma - 1}\left(1 - \left(\frac{\mathrm{P_r}}{P_d}\right)^{\frac{\gamma-1}{2\gamma}}\right) \tag{5}$$

$$P_r = 1.62\rho_e VOD^2\left(\frac{\rho_r V_p}{\rho_e VOD}\right)^{0.25} \quad kbar \tag{6}$$

$$V_r = C_o + su_r \tag{7}$$

C_o and s are Hugoniot parameters. From the experiments, it was observed that shock velocity was linear to particle velocity. The constant C_o is the bulk sound speed in rock (km/s) or the y-intercept and s (dimensionless) is the slope (Cooper, 1996). The value of s can be estimated from the material with similar physical and chemical properties such as crystal structure, density, and chemical formation. Hugoniot slope for a variety of rocks ranges from 1.0 to 1.7, and for sulphide minerals s can be considered 1.4 (Liu & Katsabanis, 1993).

The initial rock pressure (P_o) and particle velocity (u_o) before the shock wave are assumed zero. If ρ_r is rock density, the shock wave pressure in the rock interface P_r can also be estimated from conservation of momentum in Equation (3) as shown in Equation (8);

$$P_r = \rho_r V_r u_r \tag{8}$$

The radius of the crushed zone is a function of the induced shock pressure, confinement, and dynamic compressive strength of the rock. Hino (1956) suggested that the shock wave produced by the charge could be divided into two parts; a crushing shock wave that prevails in the crushed zone and a stress wave beyond the crushed zone. Peak pressure decay occurs rapidly in the shock wave and acts over a short range. Peak pressure, P_{ir} at a distance from the charge can be estimated from equation (9).

$$P_{ir} = P_r\left(\frac{r_o}{R}\right)^{\alpha} \tag{9}$$

Where r_o is the radius of charge cross-section, R is the distance from the charge, α is the wave attenuation index for the cylindrical charge, which is assumed to range from 2 to 3 close to the charge. Sun (2013) presented modified expressions used by Dai (2002) to estimate the attenuation index in shock wave zone (α_1) and stress wave zone (α_2) as shown in Equations (10) and (11).

$$\alpha_1 = 2\left(1 + \frac{v}{1 - v}\right) \tag{10}$$

$$\alpha_2 = 2\left(1 - \frac{v}{1 - v}\right) \tag{11}$$

The change from plastic deformation in the crushed zone to elastic deformation in the fracture/crack zone by stress waves can be explained by the Hugoniot Elastic Limit (HEL) concept, which is based on the decrease in amplitude of shock waves. Rosenberg (1993) developed a

relationship between Hugoniot Elastic Limit stress (σ_{HEL}) and the dynamic compressive strength of the rock (σ_{cd}) in Equation (12).

$$\sigma_{HEL} = \frac{1-v}{(1-2v)^2}\sigma_{cd} \tag{12}$$

3. Estimation of Damage Zones

To estimate damage zones around the blasthole, the equations and steps illustrated with a flowchart in Figure 2 are applied. Fundamental aspects of this work include estimation of blast energy from VOD measurements and blast energy-rock mass interaction through vibration monitoring to determine the energy attenuation and therefore estimate the sizes of damage zones around a blasthole and the extent of useful energy. The assumption in this section is the rock is isotropic with uniform distribution of flaws and micro-cracks. In the last section, further analysis of the effects of structures is discussed.

VOD measurement is conducted in the field to determine detonation pressure, P_d (Pa), which is estimated from explosive density, ρ_e (kg/m^3), and *VOD* (m/s) from the expression in Equation (13). It should be noted that Equation (13) to Equation (19) in this discussion are referenced from equations in Figure 2. Detonation pressures impinging on the borehole wall (P_b) for a fully coupled hole have been estimated at 45% to 50% of the theoretical detonation pressure (ISEE, 2011). A more recent analysis by Barreto (2020) indicates that this value can be as low as 15% under non-ideal detonation behavior in rock masses. In this case, a 50% ratio is used in estimating borehole pressure.

Prior researches indicate the ratio of the crushed zone to borehole radius ranges from 2 to 5 (Brady & Brown, 2006; Hustrulid, 1999; Liu & Katsabanis, 1993). Esen et al. (2003) suggested that the radius of the crushed zone is a function of blasthole radius (r_o), borehole pressure (P_d), and dynamic properties of rock. From the analysis of 92 blasting tests on the concrete of variable strength, they established a model to predict the radius of the crushed zone (r_c) in Equations (14) and Equation (15). K is concrete (intact rock) stiffness (Pa), σ_c is the uniaxial compressive strength (Pa), E_d is the dynamic Young's modulus (Pa) and v_d is the dynamic Poisson's ratio. Although the approach was developed using concrete, which is a man-made material with different conditions from the rock mass, validation of results has demonstrated its applicability to production blasting. These equations are used to estimate the crushed zone radius from measured VOD and dynamic rock strengths and elastic constants.

The pressure experienced at the limit of the crushed zone, Peq, may be estimated from a peak pressure attenuation function developed by Liu and Katsabanis (1993). P_{eq} as seen in Equation (16) is derived from borehole pressure P_b, borehole radius r_o, the radius of pulverized zone r_c, and pressure decay factor ϕ. The pressure decay factor is an empirical curve fitted function of the rock and explosive properties, where V_p is the p-wave velocity in the rock. This function was developed from several rock samples, including concrete, and is proved to agree with computed blast results with a standard deviation of 1.45%.

Peak particle velocity at the limit of a crushed zone, PPVeq is estimated using Equation (17) for the stress in a plane, adopted from Persson et al. (1994), who assumed that the rock is intact and continuous without any structure. This assumption can be valid under very high loading rates where the entire distribution of flaws can be activated and dependency on the weak links decreases (Kimberley et al., 2013). Attenuation characteristics of the stress waves in a rock mass beyond the crushed zone for a given explosive charge may be estimated by a square root scaled distance (SD_2) function of maximum charge mass detonated within any eight milliseconds, W (kg), and distance

between the blast centroid and monitoring point, R (m) as seen in Equation (18) (Nicholls et al., 1971). When scaled distance, SD_2, is combined with PPV monitoring, site-specific rock mass influenced empirical constants A and B may be established. A is suggested to be indicative of the type of rock mass geology, while B is the ability of vibrations to attenuate in the rock mass.

Forsyth (1993) presented an expression to determine the critical PPV that can induce fresh tensile fractures in a rock mass given the rock mass 'pseudo' elastic properties in Equation (19), where PPVcr critical PPV, above which the rock mass would prospectively fail by tension (mm/s). σ_T is the uniaxial tensile strength of rock (Pa), $\mathcal{E}_{T\text{-}cr}$ is the critical tensile strain (mm/mm), and E is the Young's Modulus (Pa). The use of Young's modulus in tensile failure, which assumes that the rock is homogeneous and deriving tensile strength and fracture mechanism under quasi-static unconfined conditions are the two inherent flaws in this expression. To rectify this, dynamic properties of the rock have been estimated and used to reflect blast experienced strengths.

4. Case Study - Nyankanga Pit Geita Gold Mine

The approach proposed was implemented at Nyankanga Pit, Geita Gold Mine (GGM). The Nyankanga geology comprises a banded iron formation (BIF) and diorite as host rocks. Mineralization is controlled by tectonic structures located within fault zones passing through the host rock. The banded iron formation is a sedimentary cyclic depositional origin consisting of iron-rich sediments and chert. The diorite is igneous with variable mineral composition and grain size defining the Nyankanga Intrusive Complex. The principal composition of the Nyankanga diorite is plagioclase-rich diorite (DPH) and hornblende-rich diorite (DHP). Porphyry intrusions within the fault zones are the youngest Nyankanga geology. The intrusions are mainly feldspar porphyry (FP) and Quartz feldspar porphyry (QFP) dykes. Lithology mapping conducted on the studied benches 920 RL to 910 RL in Nyankanga pushback 8, identified the rock distribution as shown in Figure 3. The rock quality designation (RQD) was estimated using (Deere & Deere, 1988) approach from the core samples of sizes NQ (47.6 mm) and HQ (63.5 mm). The orientation of drill holes ranges from 52° to 79° dip and 178° to 196° azimuth.

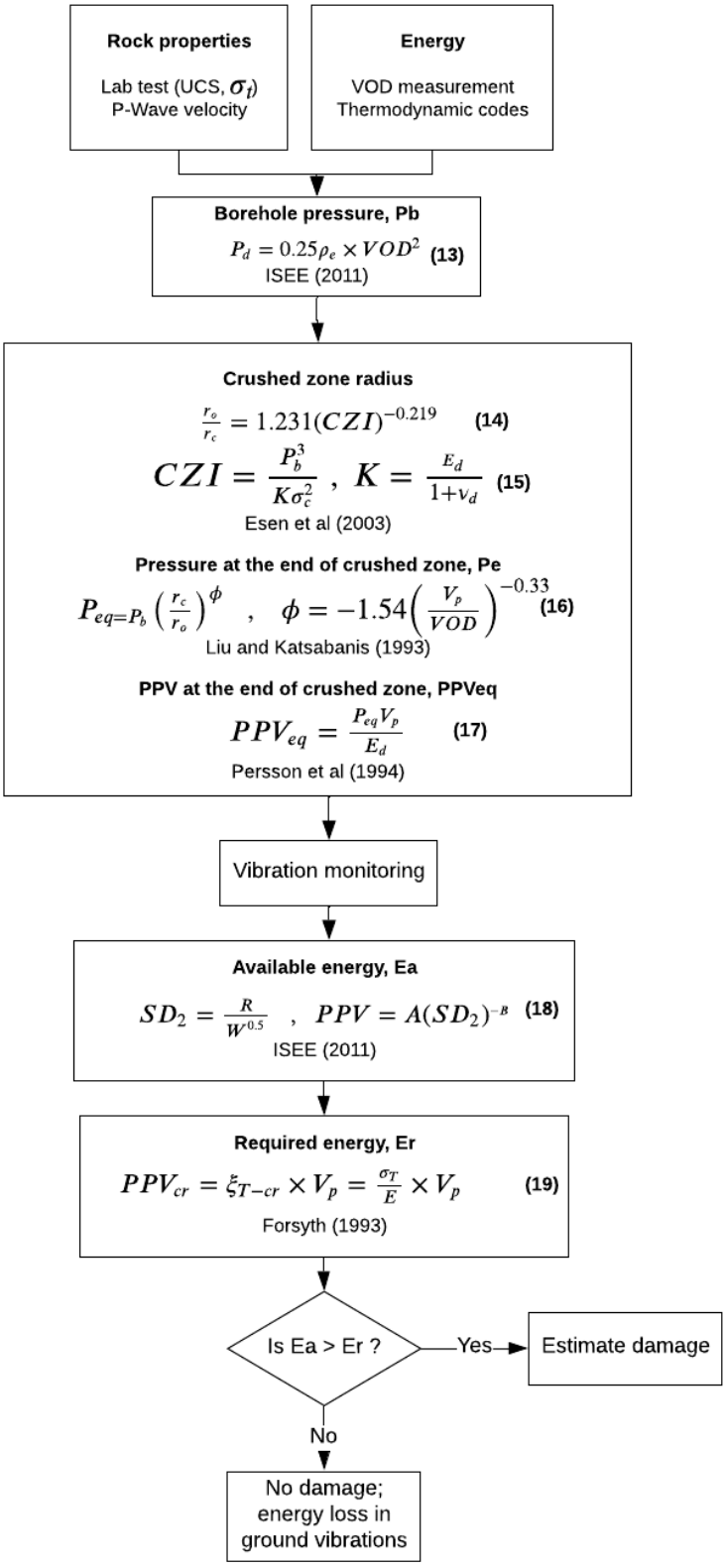

Figure 2. Blast damage analysis process.

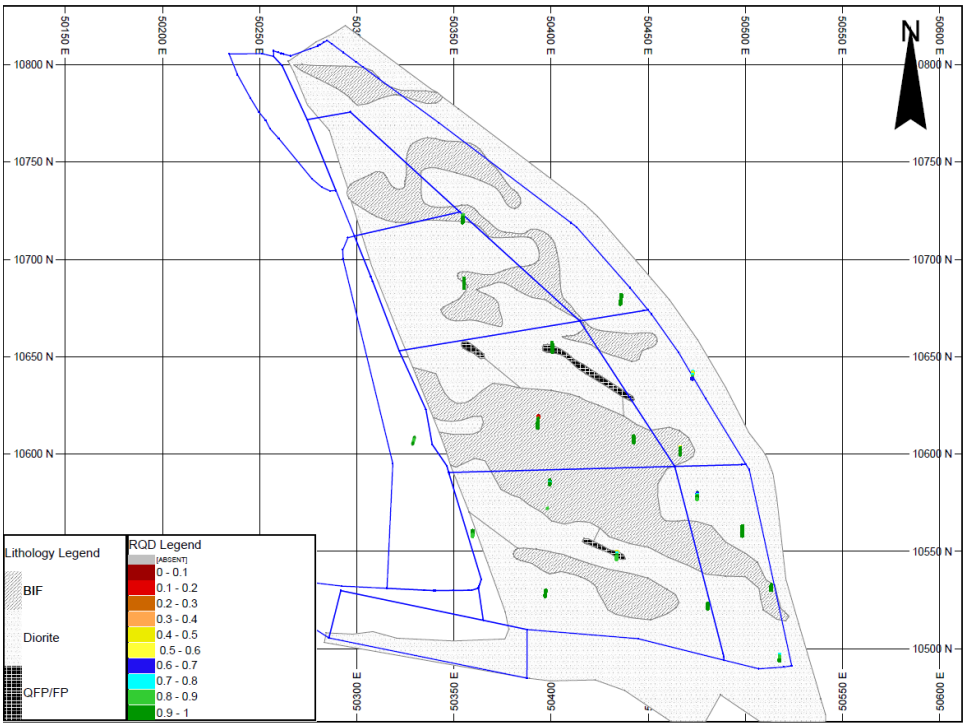

Figure 3. Nyankanga Pit Bench 920_910 lithology.

Nyankanga rock mass is categorized as a good rock made up of hard rock with uniaxial compressive strength (UCS) ranging from 78 to 129 MPa, slightly rough joints spaced 0.2 to 0.42 m with joints apertures less than 5 mm. The groundwater condition is generally moist, with water dripping in few areas. Table 1 presents the physical properties of the rock types in Nyankanga, and Table 2 the RMR estimated from the UCS, RQD, joints spacing (J_{sp}), joint condition (J_c), and ground water condition (G_w) using Bieniawski (1989) approach. The wall points (P_1 to P_{13}) are the middle points with a span distance ranging from 9 to 15 m. From each of these sections, wall mapping was conducted for RMR estimation to characterize the rock mass. It should be noted that most Nyankanga Pit structures strike NNW-SSE at an average dip direction of 255° and dip angle of 64°. The firing direction is in the SW direction almost perpendicular to the structural orientation as shown in Figure 4, which according to Ma and An (2008), does not favor further fracturing from reflected waves.

Table 1. Description of mechanical properties.

Rock type	DPH	DHP	BIF	FP/QFP
Brazilian Tensile strength, MPa	-	15.21± 2.15 (4)*	14.16 ± 2.13(4)*	-
UCS, MPa	46.36 ± 8.03 (4)*	110.39 (2)*	126.02 ± 8.03 (7)*	-
Young's modulus, GPa	76.73	-	90.83	-
Poisson's ratio	0.25	-	0.24	-
Maximum sonic speed, m/s	6,300	6,200	5,880	5,960
Mean sonic speed, m/s	4,683± 164 (65)*	5,089± 190 (83)*	4,369± 251 (34)*	4,481± 324 (27)*
Rock density, t/m^3	2.62	2.90	2.67	-

()* Number of samples tested, DPH – Plagioclase rich diorite, DHP – hornblende rich diorite, BIF – banded iron formation, FP – felsic porphyry, QFP is Quartz rich porphyry

Table 2. RMR classification.

Wall Points	Rock type	UCS (MPa)	RQD (%)	J_{sp} (mm)	J_{sp} rate	J_c rate	G_w rate	RMR
P_1	BIF	126	81	417	10	24	7	70
P_3	DPH/BIF	86	85	296	10	20	7	61
P_5	DPH/BIF	86	85	296	10	21	10	65
P_7	DPH	78	89	247	10	18	10	62
P_9	DPH/BIF	86	85	221	10	20	10	64
P_{11}	DPH	78	89	210	10	18	15	62
P_{13}	DPH/BIF	86	85	345	10	20	10	64

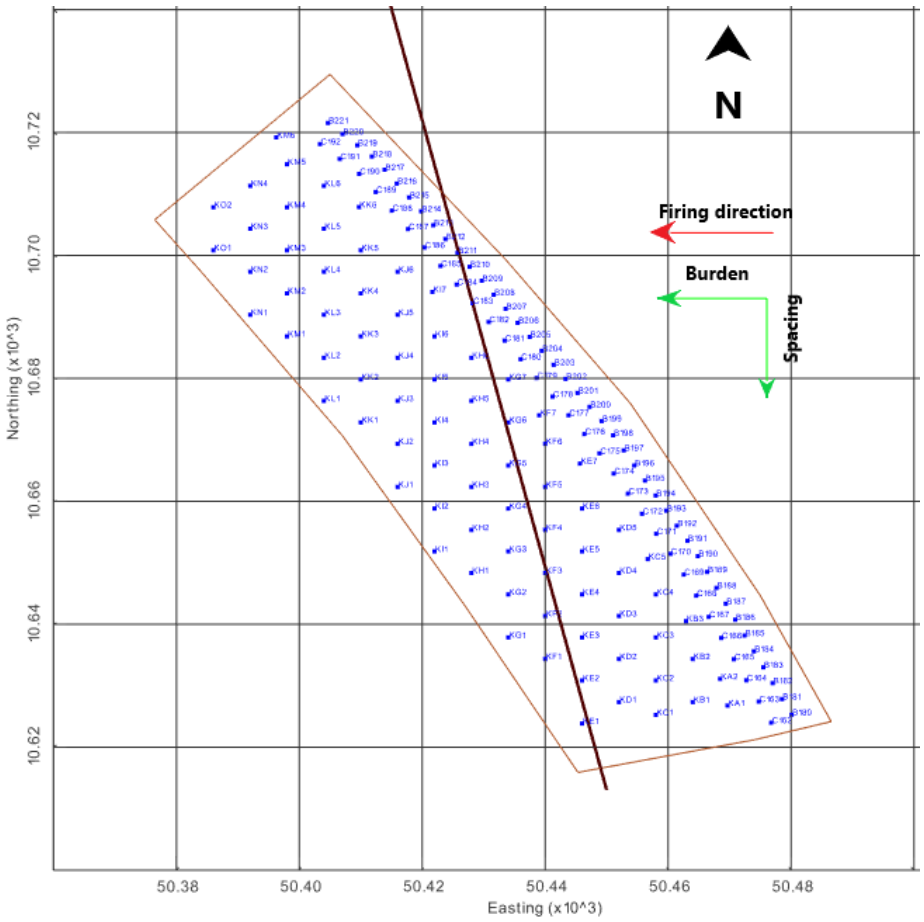

Figure 4. Structural orientation vs firing direction.

The arrangement of blasthole rows in a shot includes a pre-split line followed by the two rows of buffer holes for wall control, and then production blastholes which is a larger portion of the shot. The blastholes are drilled vertically in a staggered pattern and charged with a specially manufactured emulsion by ORICA; Fortis extra with properties summarized in Table 3, (ORICA, 2018). Detailed pattern parameters are presented in Table 4.

Blast monitoring involved measurements of VOD and ground vibrations. VOD measurements were done using MREL's MicroTrap Data Recorder, which operates under constant resistance wire

theory. A constant current is supplied to known resistance wire and upon detonation; change in resistance indicates explosive reaction. Since the constant current is supplied, a voltage drop indicates the distance initiated, and with the time, the VOD is calculated. The VOD measurement was taken from a 203 mm diameter dry hole with a 7.5 m charge column height and 4.5 m stemming height. The machine was triggered at 0 ms with the booster response spike and steady VOD measured between 11 and 13 ms, indicative of 4,401.5 m/s.

Table 3. Explosive properties.

Explosive property (units)	Value
Density (g/cm^3)	1.10 – 1.25
Minimum diameter (mm)	64
VOD (km/s)	4.1 – 6.7
Relative Effective Energy (REE), (%)	151 - 189
Bulk Energy (MJ/kg)	3.47 – 4.35 (at 1.18 g/cm^3)
Priming	Electronic detonators (I-kon)
Booster	Trojan 400 g boosters
Hole-to-hole delay (ms)	2 - 8
Row-to-row delay (ms)	100

Table 4. Blast design parameters.

Parameter (unit)	Symbol	Pre-split	Buffer 1	Buffer 2	Production
Hole diameter (mm)	D	127	127	203	203
Burden (m)	B	1.3	3.5	3.5	5.5
Spacing (m)	S	1.2	3	4.5	6.5
Bench Height (m)	H	10	10	10	10
Sub-drilling (m)	S_d	1.2	1.2	1.5	1.5
Hole depth (m)	H_d	11.2	11.2	11.5	11.5
Stemming length	S_l	-	6.5	6	4.5
Explosive density(kg/m^3)	ρ_e	-	1,180	1,180	1,180
Maximum instantaneous charge (kg)	W	15	73	210	267
Powder factor (kg/m^3)	PF	-	0.70	-	0.75

Instantel Micromate, commonly used in far-field monitoring was used to monitor vibration and air overpressure at variable distances as shown in Table 5. Data recorded over five production shots indicated wave perpendicular velocity components in longitudinal (Long), transverse (Trans), and vertical (Vert) directions measured in mm/s. The sampling frequency was set to 2,048 samples per second with a lower-end trigger level set at 5 mm/s. The seismograph also recorded wave frequencies (Hz) or duration of vibration (s), peak accelerations (g), and air overpressure level in (Pa) for each event. The geophone recording range is limited to 254 mm/s and the air overpressure (air blast) microphone to 500 Pa.

Based on the Office of Surface Mining, (OSM), among the measured particle orthogonal velocities, the component with the greatest amplitude is reported as the peak particle velocity (PPV). In this case, as far as blast damage is concerned the peak particle velocity considered is the peak vector

sum (PVS) of the three components. The results obtained are filtered and a relationship between SD_2 and particle velocity PVS as PPV is derived as shown in Figure 5. The correlation coefficient of the best fit is 0.86 which indicates a strong correlation between PVS and scaled distance. The Micromate analyzes frequency ranging from 2 to 250 Hz. The dominant frequency is defined, which is the frequency with the maximum amplitude over the whole frequency range. In this case, the Fast Fourier Transform (FFT) frequency for each channel ranged from 19 to 55 Hz at a distance range of 122 to 225m. For shot 910_3 and shot 920_6 the waveforms were not calculated, which could be due to the complex nature of the waveforms or large offset values, (Instantel, 2015).

Table 5. Vibration monitoring distance.

Shot number	Distance (m)	Charge size (kg) (in 8ms delay)	SD_2 ($m/kg^{0.5}$)	PPV (mm/s)	Overpressure (Pa)
910_3	82.82	553.0	3.52	110.20	> 500
910_4	122.13	553.0	5.19	71.77	> 500
910_5	206.93	553.0	8.80	47.03	219.4
910_6	225.26	1,106.0	6.77	21.48	493.8
920_6	550.49	276.5	33.11	8.52	365.6

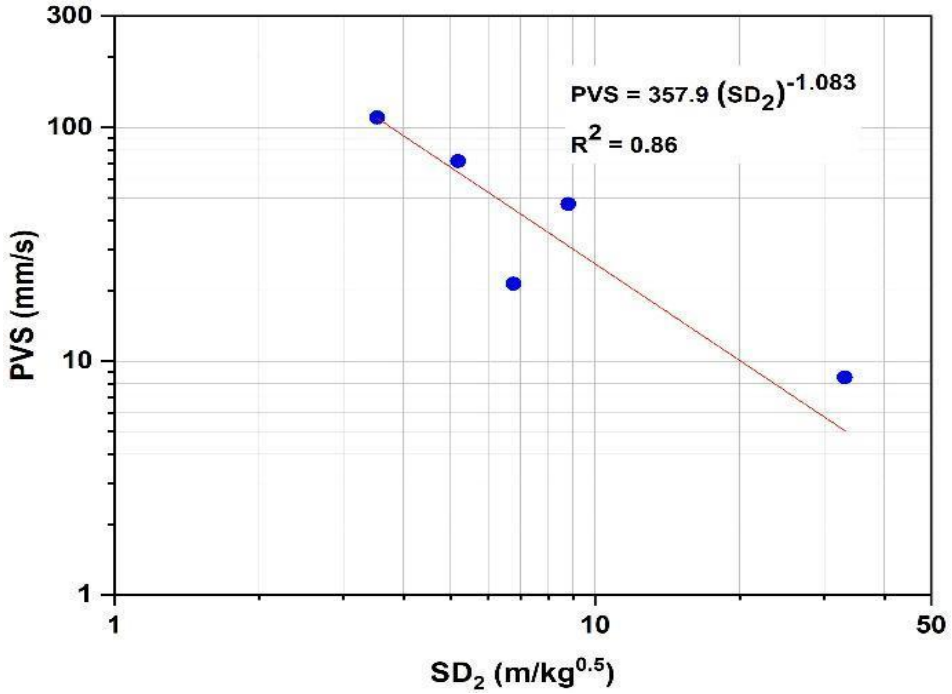

Figure 5. Particle velocity attenuation with scaled distance.

4.1. Damage Analysis

Fragmentation mechanisms in blasting can be categorized into two groups; (i) the crushed zone close to the borehole which is influenced mainly by the rock compressive strength and borehole pressure, and (ii) the region beyond the crushed zone, which is influenced predominantly by tensile failure and pre-existing in-situ fractures. The radius of the crushed zone, r_c is estimated from the measured VOD and borehole pressure in Table 6 to be 161.24 mm, which is 1.6 times the blasthole radius.

Table 6: Blast zones input parameters

Parameter (Unit)	Value
VOD (m/s)	**4,401.5**
ρ_e (kg/ m3)	**1180**
E_s (GPa)	**83.78**
ν	**0.26**
V_p (m/s)	**5,755**
ρ_r (kg/m3)	**2,780**
UCS (MPa)	**113.60**
r_o (mm)	**101.50**
σ_T (MPa)	**13.68**

While dynamic Young's modulus was estimated using Equation (20), (Eissa & Kazi, 1988), the known static Poisson's ratio was used in the absence of a dynamic Poisson's ratio being apparent at this time. It was previously observed by Heerden (1987) that, there is no consistent relationship between dynamic Poisson's ratio and static Poisson's ratio.

$$\log E_d = 0.02 + 0.77 \log\left(\rho_r E_s\right) \tag{20}$$

Peak particle velocity at the limit of the crushed zone is estimated from the experienced pressure at the end of the crushed zone. The critical peak particle velocity is assumed to occur at the mid-point of the charge and thus independent of charge length. The pressure at the limit of the crushed zone, P_e is calculated from the estimated peak pressure attenuation function and was obtained to be 1,488.13 MPa. Other estimated values are shown in Table 7.

Table 7. Blast zones results.

Parameter (Unit)	Value
P_d (MPa)	5,715.09
P_b (MPa)	2,857.55
Ed (GPa)	106.55
K (MPa)	84,565.95
CZI	21.38
r_c (mm)	161.24
ϕ	-1.41
Pe (MPa)	1,488.13
PPV_{cr} (m/s)	77.90
PPV_{dy} (m/s)	1.21

The obtained crushed zone radius and PPV at the end of the crushed zone are compared with results from Hugoniot Elastic Limit (HEL) in Equation (12), the shock wave transfer (SWT) approach by Sun (2013) in Equations 9, 10 and 11, and the site monitoring as presented in Table 8. It is observed that the results obtained offer a good comparison with the other approaches with the percentage error within 15% for the crushed zone radius and within 12% for the PPV at the end of

the crushed zone. It is further observed that far-field monitoring underestimates PPV close to the charge. Beyond one meter from the blasthole, far-field measurements offer a good comparison with SWT as seen in Figure 6.

Table 8. Crushed zone parameters comparison.

Approach	r_c (m)	Pe (MPa)	PPV (m/s)
Study approach	0.161	1488.13	77.90
SWT	0.185	1683.94	105.25
HEL	0.164	912.15	80.47
Far-field monitoring	0.161*	510.79	54.32

*Assuming the crushed zone radius similar to the study approach

Vibration monitoring data and rock's dynamic tensile strength were used to estimate the damage beyond the crushed zone limit, (CZL). From the range reported by Mohanty (1987) and Cho et al. (2003), the minimum dynamic tensile strength of two times static tensile strength was used in this case to estimate the fracture zone limit (FZL). Using Forsyth expression and dynamic input parameters in Table 6, the critical peak particle velocity in the dynamic tensile fracture zone, PPV_{dy} is obtained as 1.21 m/s equivalent to 5.4 m burden distance. Beyond this region, in the influenced zone no fracturing occurs, the wave induces incipient damage and swelling and later lost as ground vibrations. The limits of damage zones relevant in fragmentation are illustrated in Figure 6.

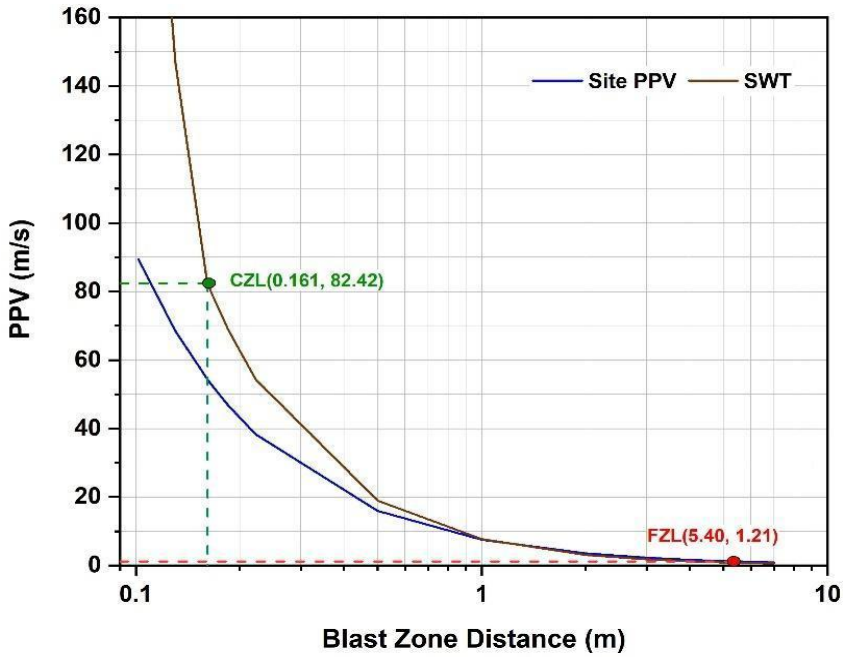

Figure 6. Damage zones.

4.2 Fragmentation Analysis

Fragmentation size analysis was performed using Wip-frag software capable of picture taking and analyzing fragment size from the blasted muckpile. All pictures were taken once after blasting on a single point on top of the muckpile. Usually, oversize on top of the muckpile can be expected due

to excessive stemming or toe problem from the upper bench which was not the case in the study area and still distinctive variation in fragmentation could be observed along the muckpile. Blast movement observed from the tie-up plan in Figure 7 indicates material movement perpendicular to the pit wall making a comparison between intact block size with resulting fragmentation size straight ahead justifiable. The mine has set fragmentation targets to mean particle size (P_{50}) of 130 mm and 80% passing (P_{80}) of 200 mm for excavators. The crusher P_{80} feed size is 300 mm with a maximum feed size of 800 mm.

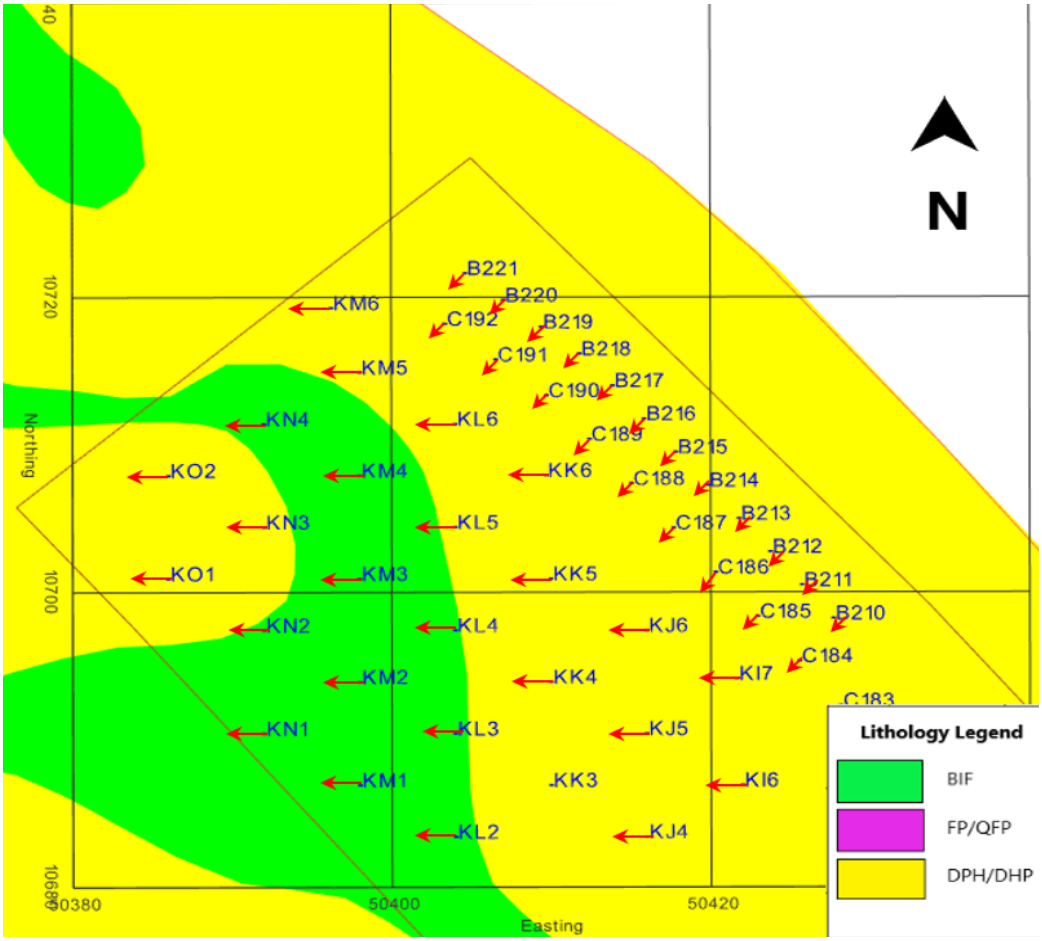

Figure 7. Blast movement on tie-up plan.

Seven pairs of data for in-situ block size and resulting fragmentation were taken from the locations shown in Figure 8 and analyzed. The insitu block size was estimated using Wang's equation method (Wang et al., 1990) using a series of steps as described by Latham et al. (2006) from the discontinuities spacing distributions, persistence, orientation, and the number of sets. From the fragmentation analysis, P_{50} is the average fragment size. The ratio of intact block size to muckpile fragment size (P_{50}) is presented as block reduction factor (BRF). Variations of BRF along the burden and from energy/rock mass interactions are illustrated in Figure 9 from the computations in Table 9.

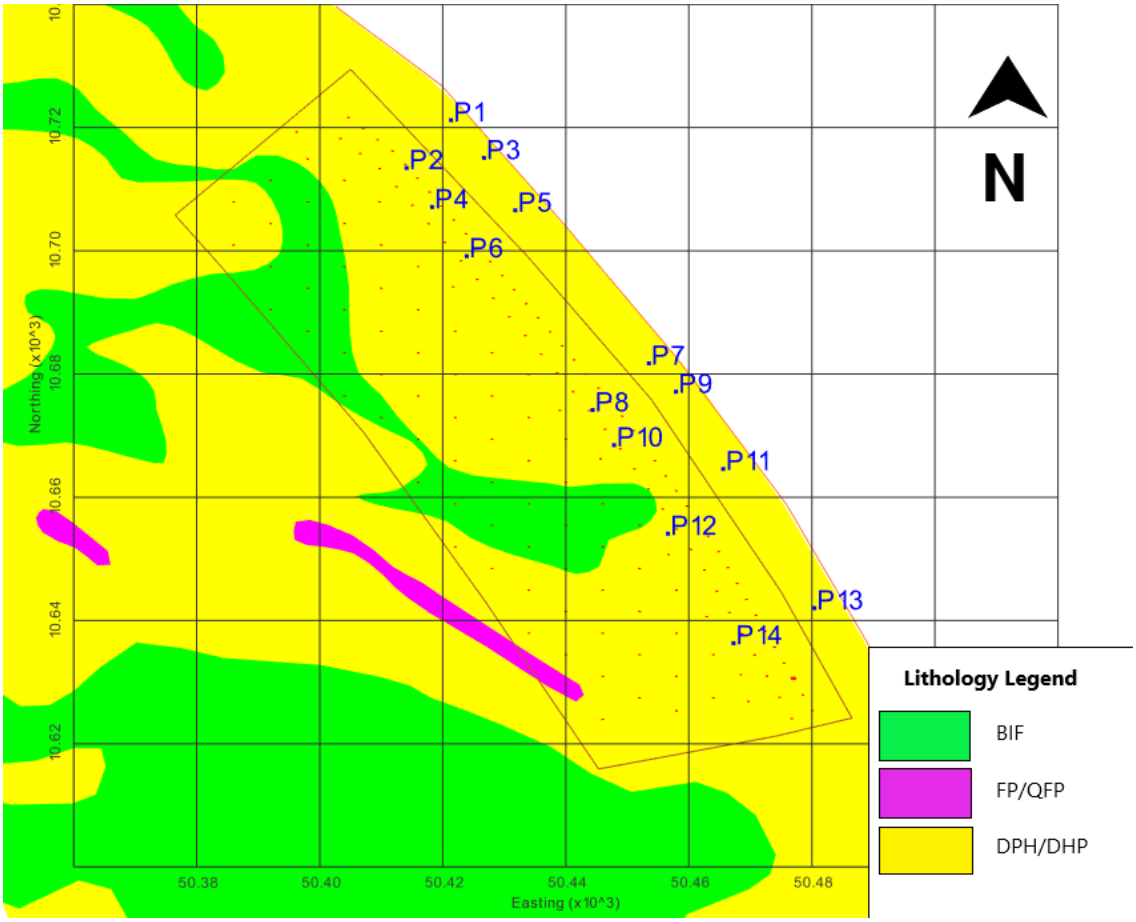

Figure 8. Locations of wall and muckpile images.

Table 9. RMR with block reduction factor analysis.

Muckpile Point	Distance from BH, m	Intact rock size (B_{50}), (m)	RMR	Charge, kg	SD (m/kg$^{0.5}$)	PPV (m/s)	Average frag. (P50)	PPV * RMR	BRF (B50/P50)
P2	2.48	1.04	70	73.24	0.29	1.37	129.14	0.96	8.09
P4	2.17	1.68	61	73.24	0.25	1.58	237.42	0.96	7.07
P8	0.8	0.67	62	210	0.06	8.25	73.67	5.11	9.12
P6	2.8	2.38	65	210	0.19	2.12	267.09	1.38	8.89
P10	1.27	2.26	64	210	0.09	5.00	103.97	3.20	21.72
P12	1.65	1.42	62	210	0.11	3.76	87.98	2.33	16.16
P14	1.99	1.30	64	210	0.14	3.07	184.40	1.97	7.07

The plot of BRF against burden distance (blue) in Figure 9 indicates no clear trend between BRF and burden distance, although it is expected that the block reduction factor would decrease with burden distance, meaning more fragmentation should happen close to the charge. The lack of a clear trend implies that other factors than the distance from the charge influence the fragmentation process. Considering the RMR and PPV as input parameters to achieve block reduction factor (red), no clear trend is also observed.

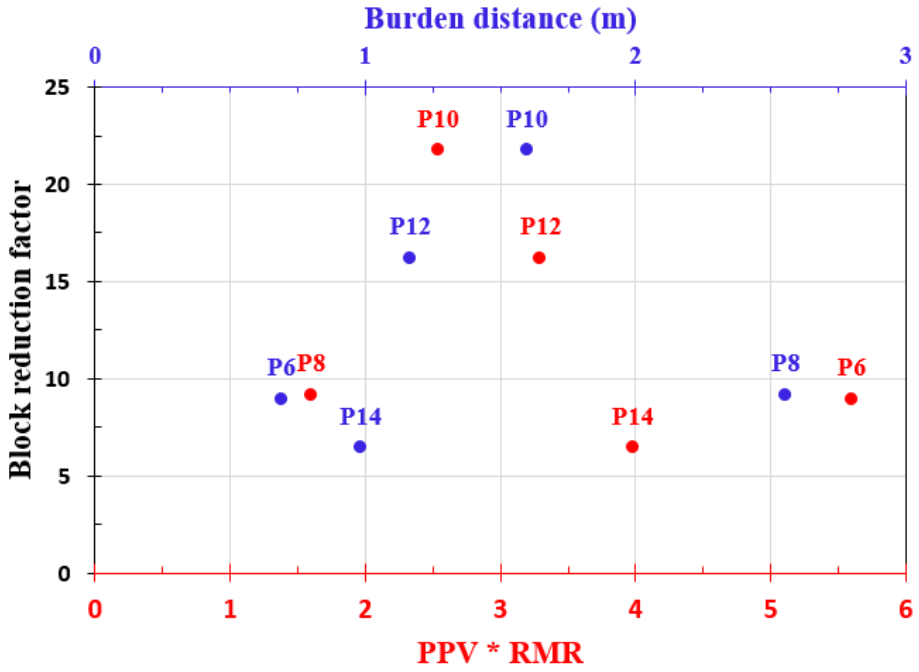

Figure 9. Block reduction factor analysis along the burden distance (blue) and variable energy and RMR (red).

5. Discussion and Conclusions

Rock mass properties have a major influence on blast energy distribution, usage, and overall blast results. Through VOD measurement, vibration monitoring, and fragmentation analysis, the interaction between blast energy and the rock mass was analyzed in two ways: how the energy attenuates within the rock mass and the variability of fragmentation with the burden distance. From preliminary data collection and analysis, it has been indicated that the wave energy attenuates at a rate described in Figure 5. Such attenuations are accurate in a more uniform rock mass.

Fragmentation around the charge does not only depend on the size of the burden and the amount of charge detonated in the blast hole as seen in Figure 9. The variability in the intact rock and structural properties of the rock mass within the burden distance can vary fragmentation significantly. In this particular case, from the wall mapping, several joints observed intersecting the shot can explain less fracturing in locations P6, P8, and P14 as shown in Figure 10. In P_{10} and P_{12} where no major structures are observed, a higher BRF is observed.

The use of RMR to characterize the rock mass for blasting did not yield valuable explanations for fragmentation variability in this study. This can be due to the narrow range of RMR used or due to the RMR ratings not having the same influence on the blast outcomes. RMR ratings were established for stability analysis in tunnels, slopes, and foundations. Although it has great use in mines, not all the parameters and ratings necessarily have the same influence in blasting. Further analysis of the structural properties of the rock mass (joint spacing, orientation, width, and infilling material) in combination with the physical and mechanical properties of the rock (density, strength, and elastic properties) is required to define a rating system more suitable for blasting use. The analysis should target the isolation of various rock properties to determine the effect of each on blast energy usage and attenuation.

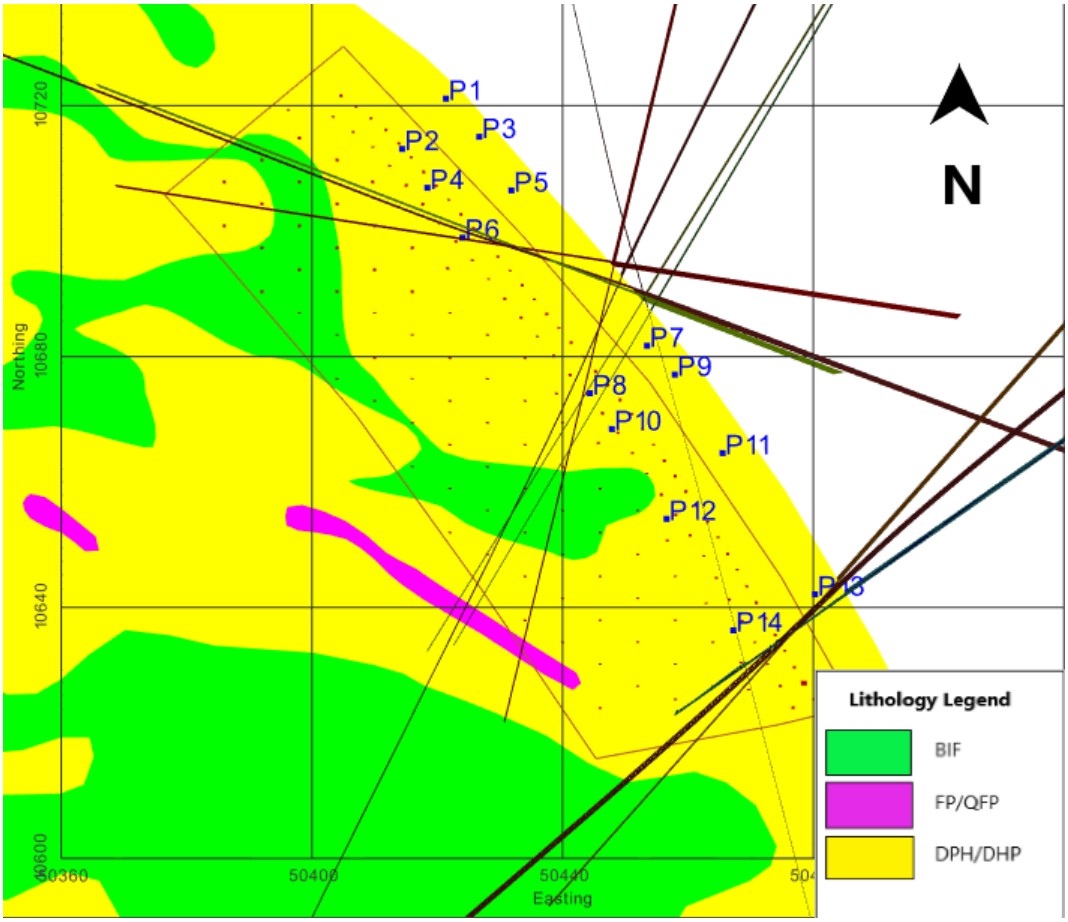

Figure 10. Mapped major structures on the pit wall.

In this case study, the designed burden was 5.5 m. From the preliminary assessment, the crushed zone is estimated to be 0.161 m and the fractured zone extends up to 5.4 m which are solely formed by the action of induced stress waves; further fragmentation can be expected from wave reflection at the free face and during the gas expansion phase. From the fragmentation size analysis, the average P_{50} is 171.6 mm, P_{80} is 340 mm and P_{100} can go up to 757 mm. While the crusher fragmentation target is easily achieved in this setting, the excavator might struggle with oversize rock. Adjustments on explosive loading and pattern size to cater for variability in rock properties can be an effective way to control fragmentation.

5. Future Work

Rock mass characteristics have a major influence on blast outcomes and should be given adequate consideration in blast design. This paper presents the analytical approach to assess the impacts of rock mass properties on blast results. The analysis shows that the structural nature of the rock mass highly impacts blast-induced fragmentation.

Further studies are suggested to isolate impacts of individual intact rock and structural properties on blast energy and resulting fragmentation to be able to customize a system to rate rock mass which will be more suitable for rock blasting. Stress wave monitoring on multiple locations targeting changes in rock properties or structures can offer a better insight into the stress levels the rock is experiencing and enable blast process modelling.

The damage zones have been estimated from available energy and loading rate-dependent rock properties, which also determine the boundary of effective wave energy (burden). Although they can be correct under the assumption that the rock is isotropic, homogeneous, and continuous, they may not be regular in heterogeneous and discontinuous rock mass as shown by variation in fragmentation in the discussion above. Field observations and modelling are required to refine predictions.

It should be noted that this study was more focused on wave energy and did not account for the effects of gas pressure. The analysis of the combined effect of wave energy and gas pressure is required to fully assess rock mass/ explosive interaction and predict blast results.

6. Acknowledgment

The authors acknowledge the support of the management at Geita Gold Mine for granting us permission to enter the mine site and collect data for the study. Special thanks to the management of ORICA (GGM), the management of Capital Drill (GGM), and all engineers, technicians, and fieldwork personnel for their involvement in this study.

7. References

[1] Ak, H., & Konuk, A. (2008). The effect of discontinuity frequency on ground vibrations produced from bench blasting: A case study. *Soil Dynamics and Earthquake Engineering, 28*(9), 686-694. doi:https://doi.org/10.1016/j.soildyn.2007.11.006

[2] Barreto, M. M. M. (2020). *An energy – Fragmentation approach for blasting performance.* (Master of Science), University of Alberta.

[3] Bieniawski, Z. T. (1989). *Engineering rock mass classifications: a complete manual for engineers and geologists in mining, civil, and petroleum engineering*: John Wiley & Sons.

[4] Bilgin, A., Esen, S., & Kılıc-, M. (1998). *The Investigation to Eliminate the Environmental Problems caused by Blasts at TKI Can Lignite Mine*. Retrieved from Ankara, Turkey:

[5] Blair, D., & Minchinton, A. (1997). On the damage zone surrounding a single blasthole. *Fragblast, 1*(1), 59-72. doi:10.1080/13855149709408390

[6] Brady, B. H. G., & Brown, E. T. (2006). *Rock Mechanics for underground mining* (Third ed.). The Netherlands: Springer, Dordrecht.

[7] Brinkmann, J. R. (1990). *An Experimental Study of the Effects of Shock and Gas Penetration in Blasting*. Paper presented at the Fragblast 90, Bisbane

[8] Chakraborty, A. K., & Jethwa, J. L. (1996). *Feasibility of air-deck blasting in various rock mass conditions - A case study*. Paper presented at the Rock fragmentation by blasting: Proceedings of the Fifth International Symposium on Rock Fragmentation by Blasting FRAGBLAST 5, Montreal, Quebec, Canada.

[9] Chitombo, G. P., Guest, A., Djordjevic, N., & La Rosa, D. M. (1999). *In search of an improved understanding of the fundamentals of rock breakage under controlled dynamic loading*. Paper presented at the Fragblast 1999, Johannesburg, SA.

[10] Cho, S. H., Ogata, Y., & Kaneko, K. (2003). Strain-rate dependency of the dynamic tensile strength of rock. *International Journal of Rock Mechanics and Mining Sciences, 40*(5), 763-777. doi:https://doi.org/10.1016/S1365-1609(03)00072-8

[11] Cooper, P. W. (1996). *Explosives Engineering*. New York: John Wiley & Sons Inc.

[12] Cunningham, C. (2005). *The kuz-ram fragmentation model - 20 years on.* Paper presented at the Brighton Conference Proceedings.

[13] Dai, J. (2002). *Dynamic behaviors and blasting theory of rock*. Beijing, China: Metallurgical Industry Press.

[14] Deere, D. U., & Deere, D. W. (1988). The Rock Quality Designation (ROD) Index in practice, Rock Classification systems for Engineering Purposes. *ASTM STP 98, 4American Society for Testing and Materials,Philadelphia*, 91-101.

[15] Eissa, E. A., & Kazi, A. (1988). Relation between static and dynamic Young's moduli of rocks. *International Journal of Rock Mechanics and Mining Sciences & Geomechanics Abstracts, 25*(6), 479-482. doi:https://doi.org/10.1016/0148-9062(88)90987-4

[16] Esen, S., Onederra, I., & Bilgin, H. A. (2003). Modelling the size of the crushed zone around a blasthole. *International Journal of Rock Mechanics and Mining Sciences, 40*(4), 485-495. doi:https://doi.org/10.1016/S1365-1609(03)00018-2

[17] Fleetwood, K., Villaescusa, E., & Li, J. (2009). *Limitations of using PPV damage models to predict rock mass damage.* Paper presented at the Thirty-Fifth Annual Conference on Explosives and Blasting Technique, Denver, CO, USA.

[18] Forsyth, W. W. (1993). A Discussion of Blast-Induced Overbreak in Underground Excavations, Rock. *Fragmentation by Blasting, Rossmanith (ed)*, 161-166.

[19] Hamdi, E., Bouden Romdhane, N., du Mouza, J., & Le Cleac'h, J. M. (2008). Fragmentation Energy in Rock Blasting. *Geotechnical and Geological Engineering, 26*(2), 133-146. doi:10.1007/s10706-007-9153-4

[20] Hamdi, E., & du Mouza, J. (2005). A methodology for rock mass characterisation and classification to improve blast results. *International Journal of Rock Mechanics and Mining Sciences, 42*(2), 177-194. doi:https://doi.org/10.1016/j.ijrmms.2004.07.005

[21] Hao, H., Wu, Y., Ma, G., & Zhou, Y. (2001). Characteristics of surface ground motions induced by blasts in jointed rock mass. *Soil Dynamics and Earthquake Engineering, 21*(2), 85-98. doi:https://doi.org/10.1016/S0267-7261(00)00104-4

[22] Heerden, W. L. (1987). General relations between static and dynamic moduli of rocks. *International Journal of Rock Mechanics and Mining Sciences & Geomechanics Abstracts, 24*(6), 381-385. doi:https://doi.org/10.1016/0148-9062(87)92262-5

[23] Henrych, J. (1979). The Dynamics of explosion and its use (Vol. 1, pp. 558). Amsterdam: Elsevier Scientific Publishing Company.

[24] Hino, K. (1956, 23-25 April 1956). *Fragmentation Of Rock Through Blasting And Shock Wave Theory Of Blasting.* Paper presented at the The 1st U.S. Symposium on Rock Mechanics (USRMS), Golden, Colorado.

[25] Hustrulid, W. A. (1999). *Blasting Principles for Open Pit Mining* (Vol. Vol. 1 General Design Concepts): CRC Press.

[26] Instantel. (2015). Blastware Operator Manual *714U0301* (Rev 22 ed.). Canada.

[27] ISEE. (2011). *ISEE blasters' handbook* (18 ed.). Cleveland, Ohio: International Society of Explosives Engineers.

[28] Kanchibotla, Valery, W., & Morrell, S. (1999). *Modeling fines in blast fragmentation and its impact on crushing and grinding.* Paper presented at the Explo'99: A Conference on Rock Breaking, Kalgoorlie.

[29] Kimberley, J., Ramesh, K. T., & Daphalapurkar, N. P. (2013). A scaling law for the dynamic strength of brittle solids. *Acta Materialia, 61*(9), 3509-3521. doi:https://doi.org/10.1016/j.actamat.2013.02.045

[30] Kuzu, C. (2008). The importance of site-specific characters in prediction models for blast-induced ground vibrations. *Soil Dynamics and Earthquake Engineering, 28*(5), 405-414. doi:https://doi.org/10.1016/j.soildyn.2007.06.013

[31] Latham, J.-P., Van Meulen, J., & Dupray, S. (2006). Prediction of in-situ block size distributions with reference to armourstone for breakwaters. *Engineering Geology, 86*(1), 18-36. doi:https://doi.org/10.1016/j.enggeo.2006.04.001

[32] Liu, Q., & Katsabanis, P. D. (1993). *A Theoretical Approach to the Stress Waves Around a Borehole and Their Effect on Rock Crushing*. Paper presented at the Proceedings of the Fourth International Symposium on Rock Fragmentation by Blasting-Fragblast-4, Vienna, Austria.

[33] Liu, Q., & Tidman, J. P. (1995). *Estimation of the Dynamic Pressure Around a Fully Loaded Blasthole*. Retrieved from Valda'r Quebec: https://books.google.ca/books?id=sZ1DjwEACAAJ

[34] Lizotte, Y., & Scoble, M. (1994). Geological control over blast fragmentation. *CIM Bulletin, 87*(983), 57-71.

[35] Lusk, B., & Silva, J. J. (2018). Energy Distribution in the Blast Fragmentation Process. In K. Awuah-Offei (Ed.), *Energy Efficiency in the Minerals Industry: Best Practices and Research Directions* (pp. 11-30). Cham: Springer International Publishing.

[36] Ma, G. W., & An, X. M. (2008). Numerical simulation of blasting-induced rock fractures. *International Journal of Rock Mechanics and Mining Sciences, 45*(6), 966-975. doi:https://doi.org/10.1016/j.ijrmms.2007.12.002

[37] McKee, D. J. (2013). *Understanding mine to mill* (T. C. R. C. f. O. R. Extraction Ed.). Brisbane.

[38] Mohanty, B. (1987). *Strength of rock under high strain rate loading conditions applicable to blasting.* Paper presented at the Fragblast'87, Keystone, Colorado.

[39] Mojitabai, N., & Beattie, S. G. (1996). Empirical approach to prediction of damage in bench blasting. *Trans. Inst. Min. and Metall, Sect. 105*, 75-80.

[40] Mortazavi, A., Paventi, M., Brummer, R. K., & Mohanty, B. (2002). *Modelling of blast-induced stress wave propagation and fracturing in hard rock material*. Paper presented at the Canadian Institute of Mining (CIM)-Annual Conference, Vancouver, BC, Canada.

[41] Nicholls, H. R., Johnson, C. F., & Duvall, W. I. (1971). *Blasting vibrations and their effects on structures*. Washington, DC: US Bureau of Mines.

[42] Nielsen, K., & Malvik, T. (1999). Grindability enhancement by blast-induced microcracks. *Powder Technology, 105*(1), 52-56. doi:https://doi.org/10.1016/S0032-5910(99)00117-5

[43] Onederra, I., & Esen, S. (2004). An Alternative Approach to Determine the Holmberg–Persson Constants for Modelling Near Field Peak Particle Velocity Attenuation Ã. *Fragblast, 8*, 61-84. doi:10.1080/13855140412331336151

[44] ORICA. (2018). Technical data sheet - Fortis Extra System - Africa.

[45] Ouchterlony, F. (2005). The Swebrec© function: linking fragmentation by blasting and crushing. *Mining Technology, 114*(1), 29-44. doi:10.1179/037178405X44539

[46] Personn, P. (1997). The relationship between strain energy, rock damage, fragmentation, and throw in rock blasting. *Fragblast, 1*(1), 99-110. doi:10.1080/13855149709408392

[47] Persson, P. A., Holmberg, R., & Lee, J. (1994). *Rock blasting and explosives engineering*: CRC Press.

[48] Rosenberg, Z. (1993). On the relation between the Hugoniot elastic limit and the yield strength of brittle materials. *Journal of Applied Physics, 74*, 752-753. doi:https://doi.org/10.1063/1.355247

[49] Sanchidrián, J., Segarra, P., & López, L. (2007). Energy components in rock blasting. *International Journal of Rock Mechanics and Mining Sciences, 44*, 130-147. doi:10.1016/j.ijrmms.2006.05.002

[50] Singh, S. P., & Narendrula, R. (2007). *The influence of rock mass quality in controlled blasting*. Paper presented at the 26th International Conference on Ground Control in Mining.

[51] Sun, C. (2013). *Damage zone prediction for rock blasting.* (Ph.D. Thesis), University of Utah, Salt Lake City, UT, USA.

[52] Udy, L., & Lownds, C. M. (1990). *The Partition of Energy in Blasting with Non-Ideal Explosives*. Paper presented at the Fragblast.

[53] Wang, H., P., L. J., & B., P. A. (1990, August 6-10). *In-situ block size assessment from discontinuity spacing data.* Paper presented at the Proceedings of the 6th Congress of the IAEG, Amsterdam.

[54] Wu, Y. K., Hao, H., Zhou, Y. X., & Chong, K. (1998). Propagation characteristics of blast-induced shock waves in a jointed rock mass. *Soil Dynamics and Earthquake Engineering, 17*(6), 407-412. doi:https://doi.org/10.1016/S0267-7261(98)00030-X

[55] Yang, R., Bawden, W. F., & Katsabanis, P. D. (1996). A new constitutive model for blast damage. *International Journal of Rock Mechanics and Mining Sciences & Geomechanics Abstracts, 33*(3), 245-254. doi:https://doi.org/10.1016/0148-9062(95)00064-X

[56] Yang, R. L., Rocque, P., Katsabanis, P., & Bawden, W. F. (1994). Measurement and analysis of near-field blast vibration and damage. *Geotechnical & Geological Engineering, 12*(3), 169-182. doi:10.1007/BF00426985

[57] Zhang, Q. B., & Zhao, J. (2014). A Review of Dynamic Experimental Techniques and Mechanical Behaviour of Rock Materials. *Rock Mechanics and Rock Engineering, 47*(4), 1411-1478. doi:10.1007/s00603-013-0463-y

[58] Zhu, Z., Mohanty, B., & Xie, H. (2007). Numerical investigation of blasting-induced crack initiation and propagation in rocks. *International Journal of Rock Mechanics and Mining Sciences, 44*(3), 412-424. doi:https://doi.org/10.1016/j.ijrmms.2006.09.002